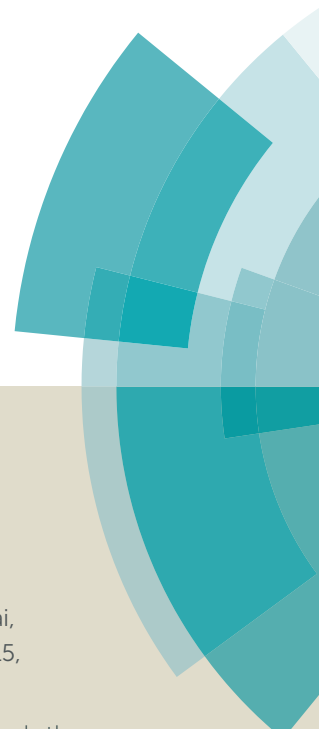
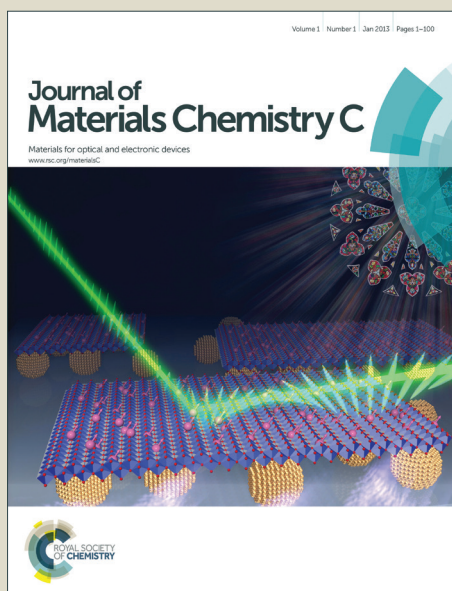


# Journal of Materials Chemistry C

Accepted Manuscript



This article can be cited before page numbers have been issued, to do this please use: Y. Li, X. Li, X. Cai, D. Chen, X. Liu, G. Xie, Z. Wang, W. Wu, C. Lo, A. Lien, J. Peng, Y. Cao and S. Su, *J. Mater. Chem. C*, 2015, DOI: 10.1039/C5TC01373A.



This is an *Accepted Manuscript*, which has been through the Royal Society of Chemistry peer review process and has been accepted for publication.

*Accepted Manuscripts* are published online shortly after acceptance, before technical editing, formatting and proof reading. Using this free service, authors can make their results available to the community, in citable form, before we publish the edited article. We will replace this *Accepted Manuscript* with the edited and formatted *Advance Article* as soon as it is available.

You can find more information about *Accepted Manuscripts* in the [Information for Authors](#).

Please note that technical editing may introduce minor changes to the text and/or graphics, which may alter content. The journal's standard [Terms & Conditions](#) and the [Ethical guidelines](#) still apply. In no event shall the Royal Society of Chemistry be held responsible for any errors or omissions in this *Accepted Manuscript* or any consequences arising from the use of any information it contains.

Journal Name

ARTICLE

Received 00th January 20xx,

Accepted 00th January 20xx

DOI: 10.1039/x0xx00000x

www.rsc.org/

## Deep Blue Fluorophors Incorporated Sulfone-Locked Triphenylamine: the Key for Highly Efficient Fluorescence/Phosphorescence Hybrid White OLEDs with Simplified Structure

Yunchuan Li<sup>a</sup>, Xiang-Long Li<sup>a</sup>, Xinyi Cai<sup>a</sup>, Dongcheng Chen<sup>a</sup>, Xin Liu<sup>a</sup>, Gaozhan Xie<sup>a</sup>, Zhiheng Wang<sup>a</sup>, Yuan-Chun Wu<sup>b</sup>, Chang-Cheng Lo<sup>b</sup>, A. Lien<sup>b</sup>, Junbiao Peng<sup>a</sup>, Yong Cao<sup>a</sup>, and Shi-Jian Su<sup>a\*</sup>

Two novel bipolar isomeric blue fluorophors, PPI-TPA-SO2-1 and PPI-TPA-SO2-2, consisting of electron-withdrawing phenanthro[9,10-d]imidazole and sulfone-locked electron-donating triphenylamine, were designed and synthesized. The sulfone lock induces more twisted molecular conformation, thus higher triplet energy level and better triplet exciton confining ability compared with the analogue TPA-PPI without the sulfone lock. In addition, the introduced sulfone lock also offers the developed materials improved electron affinities and electron dominant transporting ability. They were utilized as the blue emitter and the host for a yellow phosphorescent emitter to fabricate fluorescence/phosphorescence (F/P) hybrid white organic light-emitting diodes (WOLEDs) in a single-emissive-layer architecture, giving forward-viewing maximum current efficiencies of 44.2 and 47.6 cd A<sup>-1</sup>, power efficiencies of 49.5 and 53.4 lm W<sup>-1</sup>, and external quantum efficiencies of 14.4% and 15.6%, respectively, which are much higher than those of the devices based on TPA-PPI (29.5 cd A<sup>-1</sup>, 33.1 lm W<sup>-1</sup>, and 9.6%) due to their superior singlet and triplet exciton separation and utilization ability over TPA-PPI. These efficiencies are also the highest values ever reported for the F/P hybrid WOLEDs in a similar architecture, and their power efficiencies are even comparable with most reported highly efficient all phosphorescent WOLEDs without using any out-coupling technology.

### Introduction

Since the pioneering work by Tang et al. in 1987, extensive efforts have been devoted to promoting organic light-emitting diodes (OLEDs) into commercial applications such as flat-panel displays and lighting.<sup>1</sup> Tremendous developments of red, green, and blue OLEDs have paved the way for the recent advancements of white OLEDs (WOLEDs).

During the past two decades, various fabrication strategies based on different material systems were promoted to produce white light emission. Fully phosphorescent WOLEDs produced the highest reported efficiencies owing to the potential up to 100% internal quantum efficiency of the phosphorescent materials.<sup>2</sup> However, the lifetime of the blue phosphorescent materials hinders their commercial application in many fields.<sup>3</sup> In addition, iridium(III) bis[(4,6-difluorophenyl)-pyridinato-N,C<sup>2'</sup>]picolate (FIrpic) remains the best and most widely used blue phosphorescent emitter, which is actually a greenish blue emitter exhibiting two emission peaks centered at 472 and 500 nm.<sup>4</sup> In contrast to the phosphorescent emitter, blue fluorescent emitters can produce deep blue emission and are more stable with much longer lifetime. Therefore, a combination of blue fluorescence and phosphorescence of other

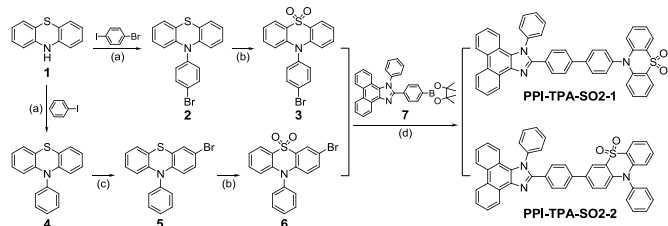
complementary colors is considered to be an ideal solution to realize high efficiency and long lifetime fluorescence/phosphorescence (F/P) hybrid WOLEDs.<sup>5a,b</sup> Besides, a blue emitter with high enough triplet energy level can give blue emission and function as the host of green/red phosphorescent emitters to realize potential 100% exciton utilization in F/P hybrid WOLEDs.<sup>6</sup> In such kind of F/P hybrid WOLEDs, the key point is to utilize the singlet and triplet excitons respectively. As triplet excitons have a much longer diffusion length (100 nm) than singlet excitons (4 nm), a spacer is generally introduced between the fluorescent and phosphorescent emission layers (EMLs) to separate the singlet and triplet excitons.<sup>5,6</sup> So these F/P hybrid WOLEDs usually consist of complicated multi-EML structures, which raise the difficulty in reproducibility and fabrication cost. Such complicated multi-EML structure is also difficult to be achieved via solution processing, which is considered to be an important process for future low-cost and large-area manufacturing.<sup>7</sup> To further simplify the F/P hybrid WOLEDs, a complementary phosphor could be doped into a blue fluorophor to form a single EML directly. Similarly, a superior singlet and triplet exciton separation and utilization ability is also requested in this case to achieve efficient utilization of the singlet and triplet excitons.

The blue emitter should not only give efficient blue fluorescence, but also has to satisfy the requirements for a phosphorescent host including high triplet energy, narrow singlet/triplet split energy ( $\Delta E_{ST}$ ), bipolar property, suitable energy levels and good thermal stability.<sup>8</sup> Much efforts have been devoted to the single-EML F/P hybrid WOLEDs. Leo et al. developed a blue fluorescent host 4P-NPD, and the WOLED based on it was reported to have a power efficiency (PE) of 10.5 lm W<sup>-1</sup> at a practical brightness of 1000 cd m<sup>-2</sup> and a maximum external quantum efficiency (EQE) of 5.5%. The limited performance was probably due to the hole dominant transporting property of 4P-NPD.<sup>9a</sup> Tao et al. demonstrated a bipolar

<sup>a</sup>State Key Laboratory of Luminescent Materials and Devices and Institute of Polymer Optoelectronic Materials and Devices, South China University of Technology, Guangzhou 510640, China Fax: +86 20 87110606; Tel: +86 20 22237098; E-mail: mssjsu@scut.edu.cn

<sup>b</sup>Shenzhen China Star Optoelectronics Technology Co., Ltd., Shenzhen 518132, China Electronic Supplementary Information (ESI) available: Thermal analysis curves, Lippert–Mataga calculations, time-resolved phosphorescent spectra, cyclic voltammograms, calculated singlet and triplet excited energies, energy level diagrams of the devices, device characteristics, and optimized molecular coordinates. See DOI: 10.1039/x0xx00000x

blue fluorescent emitter TPA-o-OXD doped with a red phosphorescent emitter to give a single-EML WOLED with a maximum current efficiency (CE) of  $7.9 \text{ cd A}^{-1}$  (a corresponding EQE of 5.2%).<sup>9b</sup> Hung et al. achieved a deep-blue fluorescence/yellow-green phosphorescence single-EML WOLED with a maximum EQE of 7% and a maximum PE of  $12.8 \text{ lm W}^{-1}$ .<sup>9c</sup> Nevertheless, these efficiencies are still far from the theoretically maximum EQE of 20%.<sup>10</sup> This situation was changed until Zhang et al. adopted DADBT as the host realizing a maximum EQE of 16.6%.<sup>11</sup> Therefore, developments of high-performance blue fluorophors as emitters as well as hosts have been considered as the current key challenges for progressing single-EML F/P hybrid WOLEDs. And all the aforementioned requirements could be satisfied only by judicious molecular design of blue emitters.



**Scheme 1.** Synthetic routes and chemical structures of the target materials PPI-TPA-SO2-1 and PPI-TPA-SO2-2. (a) 1,4-bromiodobenzene or iodobenzene, N,N-dimethylformamide (DMF), phenothiazine, copper powder, reflux; (b) dichloromethane (DCM), acetic acid, 30% hydrogen peroxide, 80 °C; (c) DCM, bromine, room temperature; (d) boronic acid ester (1.08 equiv),  $\text{K}_2\text{CO}_3$  (5.0 equiv, 2 M aq),  $\text{Pd}(\text{PPh}_3)_4$  (5 mol%), toluene/EtOH = 3/1, reflux.

A series of donor-acceptor (D-A) compounds consisting of imidazole and triphenylamine (TPA) were reported as blue fluorophors for nondoped blue OLEDs.<sup>12</sup> In this work, we introduced a new strategy of sulfone lock to develop two isomeric blue fluorophors combining phenanthro[9,10-d]imidazole (PPI) and sulfone-locked TPA units (Scheme 1). As the sulfone unit has a strong electron affinity to offer the compound good electron injection and transporting ability,<sup>13</sup> more balanced carrier recombination may be expected compared with the analogous compound without such a sulfone lock. In addition, attaching the sulfone unit between the two phenyls of TPA may give a specific molecular conformation and thus different electronic characteristics. Theoretical calculation reveals that the sulfone lock induces a more twisted molecular conformation and thus increased triplet energy level. Maximum CE values of 3.56 and  $4.80 \text{ cd A}^{-1}$ , corresponding to EQE values of 3.50% and 4.62%, are respectively achieved for the blue OLEDs with PPI-TPA-SO2-1 and PPI-TPA-SO2-2 as a nondoped EML. Moreover, F/P hybrid WOLEDs were also fabricated by utilizing PPI-TPA-SO2-1 and PPI-TPA-SO2-2 as the blue emitter as well as the host of the yellow phosphorescent

emitter iridium (III) bis(4-phenylthieno[3,2-c]pyridinato- $\text{N},\text{C}^{2'}$ )acetylacetonat (PO-01)<sup>14</sup> in a single-EML architecture, giving forward-viewing CE values of 44.2,  $47.6 \text{ cd A}^{-1}$ , PE values of 49.5,  $53.4 \text{ lm W}^{-1}$ , and EQE values of 14.4% and 15.6%, respectively. The current values are hitherto one of the highest efficiencies ever reported for the F/P hybrid WOLEDs in a similar architecture and are much higher than those of the devices based on the analogous compound TPA-PPI without the sulfone lock ( $29.5 \text{ cd A}^{-1}$ ,  $33.1 \text{ lm W}^{-1}$ , and 9.6%) due to their superior singlet and triplet exciton separation and utilization ability over TPA-PPI.

## RESULTS AND DISCUSSION

As shown in Figure S1 and Table 1, PPI-TPA-SO2-1 and PPI-TPA-SO2-2 exhibit excellent thermal stability with decomposition temperatures ( $T_d$ , corresponding to 5% weight loss) of 429 and 483 °C, respectively. In addition, a glass transition temperature ( $T_g$ ) of 189 °C was observed for PPI-TPA-SO2-2 which is much higher than that of TPA-PPI (130 °C).<sup>12b</sup> The sulfone-locked TPA offers PPI-TPA-SO2-2 more rigid molecular conformation and thus higher  $T_g$ . In contrast, no glass transition or other phase transition was found for PPI-TPA-SO2-1 in the same temperature range. Their good thermal stability and high glass transition temperature are a prerequisite for their application in OLEDs, indicating their high morphologic stability of amorphous phase in a deposited film.

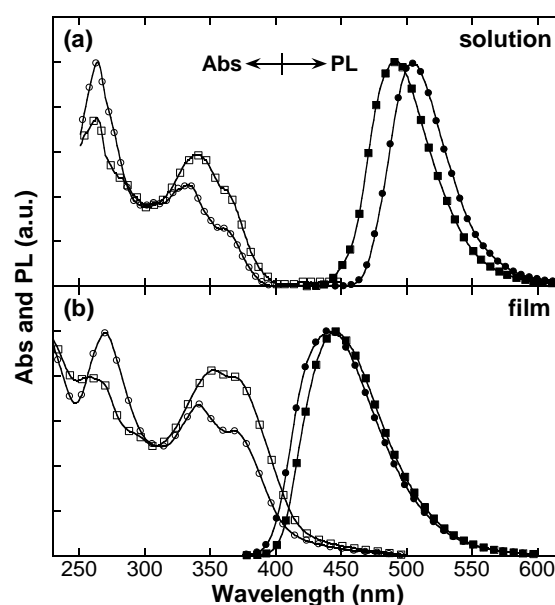


**Figure 1.** Normalized UV-vis absorption (open symbol) and PL spectra (solid symbol) of PPI-TPA-SO2-1 (○●) and PPI-TPA-SO2-2 (□■) in chloroform solution (a) and in thin solid film (b).

**Table 1.** Physical properties of PPI-TPA-SO2-1 and PPI-TPA-SO2-2

compound	$T_g^a$ (°C)	$T_d^b$ (°C)	$\lambda_{\text{abs}}^c$ (nm)	$\lambda_{\text{abs}}^d$ (nm)	$\lambda_{\text{em}}^c$ (nm)	$\lambda_{\text{em}}^d$ (nm)	IP <sup>e</sup> (eV)	EA <sup>e</sup> (eV)	$E_g^{\text{opt}}$ (eV)	$\Phi_{\text{PL}}^g$	$\Phi_{\text{PL}}^h$
PPI-TPA-SO2-1	--	429	262.2, 341.3, 365.5	270.1, 353.5, 370.8	510	439	-5.62	-2.72	2.98	0.90	0.71
PPI-TPA-SO2-2	185	483	264.3, 335.0, 363.5	259.3, 339.4, 368.6	508	446	-5.67	-2.67	2.93	0.86	0.68

<sup>a</sup>Glass transition temperature ( $T_g$ ) obtained from DSC measurements. <sup>b</sup>Decomposition temperature ( $T_d$ ) obtained from TGA measurements. <sup>c</sup>UV-vis absorption and PL spectra measured in chloroform solution. <sup>d</sup>UV-vis absorption and PL spectra measured in thin solid film. <sup>e</sup>Ionization potential (IP) and electron affinity (EA) estimated from the onset of the oxidation and reduction potentials [vs ferrocene/ferrocenium (Fc/Fc<sup>+</sup>)]. <sup>f</sup>Optical energy band gaps ( $E_g^{\text{opt}}$ ) estimated from the film absorption edge. <sup>g</sup>PL quantum yields of the DCM solutions measured using an integrating sphere ( $10^{-5} \text{ mol L}^{-1}$ ). <sup>h</sup>PL quantum yields of the thin solid films (50 nm) deposited on the quartz substrates measured using an integrating sphere.

UV-Vis absorption and photoluminescence (PL) spectra of PPI-TPA-SO<sub>2</sub>-1 and PPI-TPA-SO<sub>2</sub>-2 in dilute CHCl<sub>3</sub> solutions and in thin solid films are shown in Figure 1. The absorption features of the two compounds are similar to each other due to their homologous molecular skeleton. The absorption bands at around 270–300 nm could be associated with the  $\pi$ - $\pi^*$  transitions of the sulfone-locked TPA units, and the absorption bands in the range from 345 to 362 nm can be assigned to the  $\pi$ - $\pi^*$  transitions of the PPI moiety. Optical energy band gaps ( $E_g^{\text{opt}}$ ) are estimated to be 2.98 and 2.93 eV for PPI-TPA-SO<sub>2</sub>-1 and PPI-TPA-SO<sub>2</sub>-2, respectively, which are calculated from the threshold of the absorption spectra in films. Photoluminescence quantum yield (PLQY) in dilute dichloromethane (DCM) solution ( $10^{-5}$  mol L<sup>-1</sup>) is 0.90 for PPI-TPA-SO<sub>2</sub>-1 and 0.86 for PPI-TPA-SO<sub>2</sub>-2. In neat films (~50 nm), it is 0.71 for PPI-TPA-SO<sub>2</sub>-1 and 0.68 for PPI-TPA-SO<sub>2</sub>-2 as measured by an integrating sphere under air condition. The slightly reduced PLQY in thin solid film may be benefited from the twisted angle between the donor and the acceptor, which reduces intermolecular  $\pi$ - $\pi$  stacking efficiently to reduce the aggregation-caused quenching problem.

To distinguish the excited states of the two emitters, the PL spectra of the two emitters in various solvents with different polarities were also measured, as shown in Electronic Supplementary Information (ESI) (Figure S2). PPI-TPA-SO<sub>2</sub>-1 and PPI-TPA-SO<sub>2</sub>-2 display obvious solvatochromicity such that the emission spectrum exhibits a clear bathochromic shift (121 and 90 nm) from nonpolar solvent hexane to high polar solvent N,N-dimethylformamide (DMF). The increase of dipole moment from the ground state to the excited state was calculated from the Lipper–Mataga calculation. PPI-TPA-SO<sub>2</sub>-1 and PPI-TPA-SO<sub>2</sub>-2 exhibit a large slope of 21694 ( $R = 0.98$ ) and 19171 ( $R = 0.98$ ), respectively (Figure S3). The increase of dipole moment of PPI-TPA-SO<sub>2</sub>-1 (28.27 D) and PPI-TPA-SO<sub>2</sub>-2 (28.20 D) indicates they are in a strong charge-transfer (CT) state. A strong CT state may be of benefit to reduced  $S_1$  and  $T_1$  split energy ( $\Delta E_{ST}$ ) and exchange energy loss as a host.<sup>5</sup> In addition, an EML based on them with a small  $\Delta E_{ST}$  is extremely important to acquire a low driving voltage and a high PE in single-EML F/P hybrid WOLEDs.<sup>16</sup>

As aforementioned, higher triplet energy level ( $T_1$ ) than the phosphor is generally requested if the current blue fluorophors are used as the emitter as well as the host of the phosphor. Time-resolved phosphorescence spectra of these blue fluorophors dissolved in 2-methyltetrahydrofuran were measured at 77 K at different delayed times (Figure S4, see ESI). From the highest energy peaks of the phosphorescence spectra,  $T_1$  values are estimated to be 2.23, 2.30, and 2.30 eV for TPA-PPI, PPI-TPA-SO<sub>2</sub>-1, and PPI-TPA-SO<sub>2</sub>-2, respectively, which are equal to or higher than that of PO-01 (2.21 eV, corresponding to the emission peak). Their singlet levels are 2.82, 2.82 and 2.78 eV derived from their film emission peak. So a narrower  $S_1/T_1$  split energy (0.52 and 0.48 eV) was acquired for PPI-TPA-SO<sub>2</sub>-1 and PPI-TPA-SO<sub>2</sub>-2.

As shown in Figure S5 (see ESI), the oxidization potentials ( $E_{\text{ox}}$ ) of PPI-TPA-SO<sub>2</sub>-1 and PPI-TPA-SO<sub>2</sub>-2 were found to be 1.69 and 1.64 V. Under the same condition, ferrocene/ferrocenium (Fc/Fc<sup>+</sup>) exhibits a redox potential of 0.25 V. Note that the redox potential of Fc/Fc<sup>+</sup> has an absolute energy level of -4.8 eV to vacuum, ionization potentials (IPs) of PPI-TPA-SO<sub>2</sub>-1 and PPI-TPA-SO<sub>2</sub>-2 were estimated to be -5.62 and -5.67 eV, respectively, according to  $\text{IP} = -e(E_{\text{ox}} + 4.55)$ .<sup>17</sup> Similarly, the reduction potentials ( $E_{\text{red}}$ ) for PPI-TPA-SO<sub>2</sub>-1 and PPI-TPA-SO<sub>2</sub>-2 were found to be -1.83 and -1.88 V, and their electron affinities (EAs) were estimated to be -2.72 and -2.67 eV, respectively, according to  $\text{EA} = -e(E_{\text{red}} + 4.55)$ . Compared with the analogous compound TPA-PPI without the sulfone lock ( $\text{IP} = -5.22$  eV,  $\text{EA} = -2.27$  eV),<sup>12b</sup> simultaneously reduced IP and EA

values were achieved for the sulfone-locked compounds due to the strong electron affinity of the sulfone unit. The lower lying EA values and thus lower electron injection barrier may offer easy electron injection from the electron transport layer. In addition, the deeper IP values may improve the hole injection barrier and thus reduced hole current.

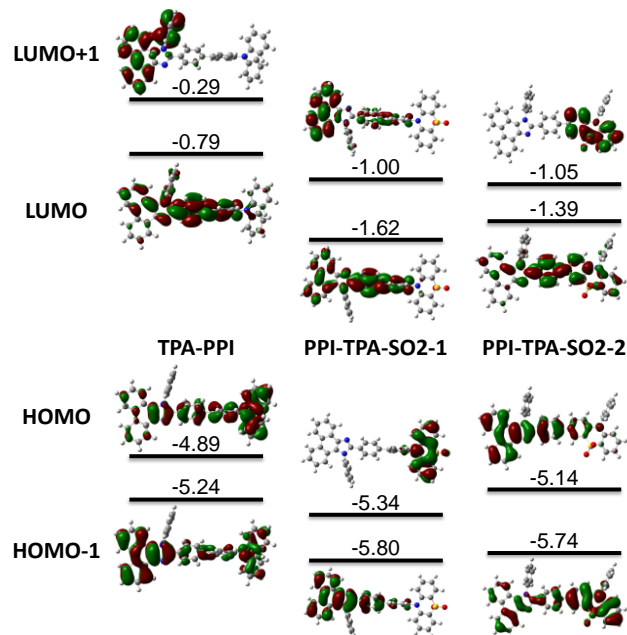


**Figure 2.** Calculated spatial distributions of HOMOs and LUMOs of TPA-PPI, PPI-TPA-SO<sub>2</sub>-1 and PPI-TPA-SO<sub>2</sub>-2.

**Table 2.** Summary of the theoretical calculations (DFT, B3LYP/6-31G (d, p) and TD-DFT, M06-2X/6-31G (d, p), Gaussian 03W)

compound	HOMO <sup>a</sup> (eV)	LUMO <sup>a</sup> (eV)	$E_g^a$ (eV)	$\mu_g^a$ (D)	$f^b$	$S_1^b$ (eV)	$T_1^b$ (eV)
TPA-PPI	-4.89	-0.79	4.10	4.15	1.72	3.84	3.06
PPI-TPA-SO <sub>2</sub> -1	-5.34	-1.63	3.71	7.49	1.23	3.95	3.08
PPI-TPA-SO <sub>2</sub> -2	-5.14	-1.39	3.75	10.44	1.59	3.91	3.06

<sup>a</sup>Calculated results of the ground state. <sup>b</sup>Calculated results of the first excited state.

To gain further insight into the structure-property relationships of the developed materials at the molecular level, quantum chemical calculations were also performed at the B3LYP/6-31G(d,p) level to investigate their ground states.<sup>18</sup> As shown in Figure 2, for TPA-PPI, the highest occupied molecular orbital (HOMO) locates on the TPA moiety, while the lowest unoccupied molecular orbital (LUMO) mostly locates on the PPI unit. Its HOMO and LUMO overlap at a long range which gives the biggest oscillator strength ( $f = 1.72$ ) among the three compounds (Table 2). The introduction of the sulfone unit endows tremendous effect on the distribution of HOMOs and LUMOs of the sulfone-locked analogues. For PPI-TPA-SO<sub>2</sub>-1, its HOMO and LUMO are obviously separated that the HOMO locates on the sulfone-locked diphenylamine moiety while the LUMO mostly located on the PPI unit. Due to the electron-withdrawing ability of the sulfone lock, the HOMO of PPI-TPA-SO<sub>2</sub>-1 was pulled towards the sulfone lock side and concentrated at the diphenylamine part. So the overlap of the HOMO and LUMO of PPI-TPA-SO<sub>2</sub>-1 was reduced and the oscillator strength of its first excited state is the smallest among the three compounds ( $f = 1.23$ ). In contrast to TPA-PPI and PPI-TPA-SO<sub>2</sub>-1, the HOMO of PPI-TPA-SO<sub>2</sub>-2 mainly locates on the PPI unit which is generally

regarded as an electron-withdrawing component while the LUMO mostly locates on the two middle benzene rings. Because the sulfone unit accesses to the entire conjugated system and has much stronger electron-withdrawing ability than imidazole, then its LUMO occurs at the place close to the sulfone unit giving a moderate oscillator strength ( $f = 1.59$ ). As their similar molecular structure, the triplet energy levels of these compounds could be affected by their dihedral angles between PPI and the sulfone-locked TPA. As shown in Figure 3, the twisted angles between the central phenyls are  $35.49^\circ$  for TPA-PPI,  $36.97^\circ$  for PPI-TPA-SO2-1, and  $-34.53^\circ$  for PPI-TPA-SO2-2, indicating the dihedral angles of PPI-TPA-SO2-1 and PPI-TPA-SO2-2 increased or reversed compared with TPA-PPI. The more twisted angles of the newly developed compounds ensure them sufficient space resistance to inhibit aggregation-caused quenching problem. Moreover, the more twisted angles may also restrain the conjugation of the backbone to give improved singlet and triplet energy levels.<sup>8</sup> Their singlet ( $S_1$ ) and triplet energy levels ( $T_1$ ) are also calculated, as shown in Table 2. The current sulfone-locked compounds have slightly higher triplet excited state energies than TPA-PPI which give positive effect as a host to fabricate F/P hybrid WOLEDs. It is also well consistent with the experimental results by the phosphorescence measurement.

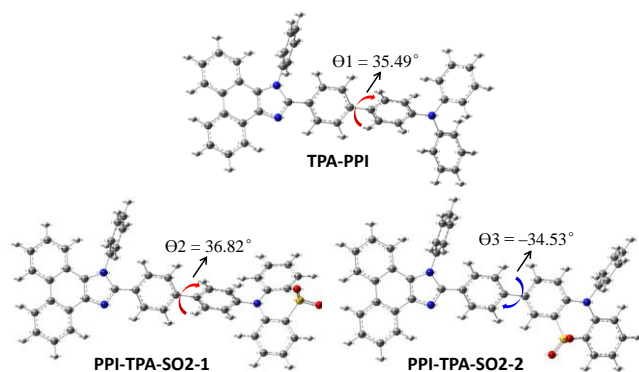


**Figure 3.** Twisted angles between the central phenyls of TPA-PPI, PPI-TPA-SO2-1, and PPI-TPA-SO2-2 based on their optimized ground states.

The excited state energies of PPI-TPA-SO2-1 and PPI-TPA-SO2-2 were calculated by M06-2X, including the first eight singlet and triplet excited states (Figure S6). The calculated exchange energy ( $\Delta E_{ST}$ ) between  $S_1$  and  $T_1$  is 0.87 and 0.85 eV for PPI-TPA-SO2-1 and PPI-TPA-SO2-2, respectively. Such a huge energy barrier between  $S_1$  and  $T_1$  is the main obstacle for up-conversion of the triplet excited state to the singlet excited state to give thermal activated delayed fluorescence (TADF).<sup>19</sup> However, the energy barriers between  $S_1$  and  $T_6$  for these two compounds are as narrow as zero. So in an electroluminescent device, it might be possible that the initially generated triplet excitons convert to the singlet excitons through reversed intersystem crossing.<sup>20</sup>

To evaluate their electroluminescent performance, a series of blue fluorescent OLEDs were fabricated with PPI-TPA-SO2-1 and PPI-TPA-SO2-2 as the nondoped EML in a structure of ITO (95 nm)/HATCN (5 nm)/NPB (40 nm)/TCTA (5 nm)/EML (20 nm)/TPBI (40 nm)/LiF (1 nm)/Al (80 nm). In this device, ITO (indium tin oxide) and LiF/Al are the anode and the cathode, respectively; NPB (4,4'-bis[N-(1-naphthyl)-N-phenyl amino]biphenyl) is the hole-transporting layer (HTL); TCTA (4,4',4''-tris(N-carbazolyl)triphenylamine) is the electron-blocking layer; TPBI serves as the electron-transporting layer (ETL) and the hole-blocking layer; and HATCN (dipyrazino(2,3-f:2',3'-h)-quinoxaline-2,3,6,7,10,11-hexacarbonitrile) was introduced as an anode buffer layer to improve the hole injection to NPB (Figure S7, see ESI). Current density and luminance versus driving voltage and current efficiency versus current density characteristics are shown in Figure S8 (see ESI). All the devices exhibited a pretty low turn-on voltage ( $\sim 2.8$  V), and the current density of the devices based on PPI-TPA-SO2-1 and PPI-TPA-SO2-2 are both improved compared with that of the device based on TPA-PPI.

As shown in Figure S9 (see ESI), all the devices exhibit quite similar electroluminescence (EL) spectra which are well consistent with their corresponding PL spectra in the thin film state and are very stable in a wide driving current density (not shown here). As shown in Table S2, at the practical application luminance of 100-1000  $\text{cd m}^{-2}$ , both PPI-TPA-SO2-1 and PPI-TPA-SO2-2 realized efficient deep blue emission, which is defined as having a Commission Internationale de l'Eclairage (CIE) coordinate  $y < 0.15$  along with  $x+y < 0.30$ . Besides, the EQE values are 3.12% and 4.67% for the devices based on PPI-TPA-SO2-1 and PPI-TPA-SO2-2, respectively, which are among the best of ever reported deep blue emitters.<sup>12</sup>

The device based on PPI-TPA-SO2-2 exhibited the highest efficiency among the devices, and it is suspected that the carrier injection and balance could play an important role.

As well-known, the upper limit of EQE is:

$$\text{EQE}_{\text{max}} = \eta_{\text{op}} \times \phi_{\text{fl}} \times \eta_r \times \gamma \approx \eta_{\text{op}} \times \phi_{\text{fl}} \times 0.25 \times \gamma \quad (1),$$

where the optical out-coupling factor ( $\eta_{\text{op}}$ ) is about 0.25-0.3, the possibility of a singlet exciton formed ( $\eta_r$ ) is 25%,  $\phi_{\text{fl}}$  is PLQY (0.84, 0.71, and 0.68 for TPA-PPI, PPI-TPA-SO2-1, and PPI-TPA-SO2-2, respectively), and  $\gamma$  is the carrier balance factor. Thus  $\gamma$  could be calculated by equation (2):

$$\gamma = 4 \text{EQE}_{\text{max}} / (\eta_{\text{op}} \times \phi_{\text{fl}}) \quad (2),$$

and the calculated  $\gamma$  values are 0.65-0.78, 0.66-0.79, and 0.91-1.09 for TPA-PPI, PPI-TPA-SO2-1, and PPI-TPA-SO2-2, respectively, indicating the device based on PPI-TPA-SO2-2 exhibits the most balanced carrier.

In order to evaluate its superior bipolar transporting property over TPA-PPI, hole-only and electron-only devices were also fabricated.

**Table 3.** Summary of the device performance of the F/P hybrid WOLEDs with TPA-PPI, PPI-TPA-SO2-1, and PPI-TPA-SO2-2 as the blue emitter as well as the host of PO-01 at 0.5 wt% doping concentration. CRI: color rendering index

Host	$V_{\text{on}}$ (V)	$\text{CE}_{\text{max}}$ ( $\text{cd A}^{-1}$ )	$\text{PE}_{\text{max}}$ ( $\text{lm W}^{-1}$ )	$\text{EQE}_{\text{max}}$ (%)	at 100 $\text{cd m}^{-2}$					at 1000 $\text{cd m}^{-2}$					CRI
					V	CE	PE	CIE	EQE	V	CE	PE	CIE	EQE	
TPA-PPI	2.6	29.5	33.1	9.67	2.9	27.1	28.3	(0.42, 0.46)	9.02	3.2	18.2	17.8	(0.40, 0.43)	6.3	43
PPI-TPA-SO2-1	2.8	44.2	49.5	14.4	3.5	34.7	35.8	(0.43, 0.48)	11.3	4.6	23.7	20.8	(0.40, 0.43)	8.2	44
PPI-TPA-SO2-2	2.6	47.6	53.4	15.6	3.2	43.2	46.9	(0.43, 0.48)	14.2	4.1	30.3	28.9	(0.40, 0.43)	10.4	44

The configuration of the hole-only devices is ITO (95 nm)/ HATCN (5 nm)/ NPB (40 nm)/ TCTA (5 nm)/ PPI-TPA, PPI-TPA-SO2-1 or PPI-TPA-SO2-2 (20 nm)/ NPB (40 nm)/ Al (80 nm), and the electron-only devices have a structure of ITO (95 nm)/ TPBI (40 nm)/ TPA-PPI, PPI-TPA-SO2-1 or PPI-TPA-SO2-2 (20 nm) / TPBI (40 nm)/ LiF (1 nm)/ Al (80 nm). As shown in Figure S10 (see ESI), though the devices based on TPA-PPI exhibit the highest hole and electron current density, the hole current density is higher than its electron current density. It could be ascribed to its large electron injection barrier from TPBI, small hole injection barrier and hole dominant transporting property. In contrast, even though the hole and electron current are both reduced for PPI-TPA-SO2-1 and PPI-TPA-SO2-2, their electron transporting ability is stronger than their corresponding hole transporting ability after TPA is locked by sulfone, indicating their electron dominant transporting property. As there is nearly no electron injection barrier from the ETL of TPBI to the EML and improved hole injection barrier, improved carrier balance could be achieved for both PPI-TPA-SO2-1 and PPI-TPA-SO2-2 especially for PPI-TPA-SO2-2.

To fabricate F/P hybrid WOLEDs, PPI-TPA-SO2-1 and PPI-TPA-SO2-2 were utilized as the blue emitter, and PO-01 with an emission peak at 560 nm was utilized as the complementary phosphor. Considering their high enough triplet energy, TPA-PPI, PPI-TPA-SO2-1, and PPI-TPA-SO2-2 were adopted as the blue emitter, meanwhile, as the host of the yellow phosphorescent emitter PO-01 to fabricate F/P hybrid WOLEDs with a single-EML configuration of ITO (95 nm)/ HATCN (5 nm)/ NPB (40 nm)/ TCTA (5 nm)/ EML (20 nm)/ TPBI (40 nm)/ LiF (1 nm)/ Al. Different from the nondoped blue OLEDs, PO-01 was doped into TPA-PPI, PPI-TPA-SO2-1 or PPI-TPA-SO2-2 in a low concentration of 0.5 wt% to give a single EML, and the 0.5 wt% PO-01 doping concentration is based on our previous work without further optimization. In this structure, singlet excitons are utilized for blue emission, and triplet excitons with much longer diffusing length excite the highly decentralized phosphorescent dopant PO-01 to give yellow emission. In an ideal situation, both 25% singlet excitons and 75% triplet excitons can be utilized in the F/P hybrid WOLEDs, leading to an unit exciton utilization and an excellent efficiency. All the devices exhibit a low turn-on voltage (<2.8 V) which is remarkable without using a p-i-n device structure and is favorable for achieving high power efficiency (Figure 4). As a result shown in Table 3, maximum forward-viewing current efficiencies of 29.5, 44.2, 47.6 cd A<sup>-1</sup>, power efficiencies of 33.1, 49.5, 53.4 lm W<sup>-1</sup>, and EQE values of 9.67%, 14.4%, 15.6% were respectively achieved for the F/P hybrid WOLEDs based on TPA-PPI, PPI-TPA-SO2-1, and PPI-TPA-SO2-2 without employing any light out-coupling technology. As illumination sources are generally characterized by their total efficiency, the maximum total PE values may reach 84.2 and 90.8 lm W<sup>-1</sup> with a general factor of 1.7 for the devices based on PPI-TPA-SO2-1 and PPI-TPA-SO2-2,<sup>5</sup> and they are hitherto among the most efficient F/P hybrid WOLEDs in a single-EML architecture, as summarized in Table S3. Besides, the power efficiencies of the F/P hybrid WOLEDs based on PPI-TPA-SO2-1 and PPI-TPA-SO2-2 are even unexpectedly higher than most previously reported highly efficient fully phosphorescent WOLEDs, as summarized in Table S4. It is worth noting that although the nondoped blue device based on PPI-TPA-SO2-1 exhibits lower efficiency than the device based on TPA-PPI, the CE value of the F/P hybrid white device based on PPI-TPA-SO2-1 is 1.5 times higher than that of the device based on TPA-PPI. Further higher CE value which is 1.6 times higher than the device based on TPA-PPI is achieved for the device based on PPI-TPA-SO2-2, and it could be attributed to the improved triplet exciton utilization in WOLEDs. In addition, the doping concentration of 0.5 wt% is so low that the triplet-triplet annihilation of the devices is minimized and the efficiency roll-off is efficiently suppressed even at high

current density. At the practical application luminance of 1000 cd m<sup>-2</sup>, the forward-viewing CE and PE values of the PPI-TPA-SO2-2 based device remain as high as 30.3 cd A<sup>-1</sup> and 28.9 lm W<sup>-1</sup> due to the reduced efficiency roll-off.

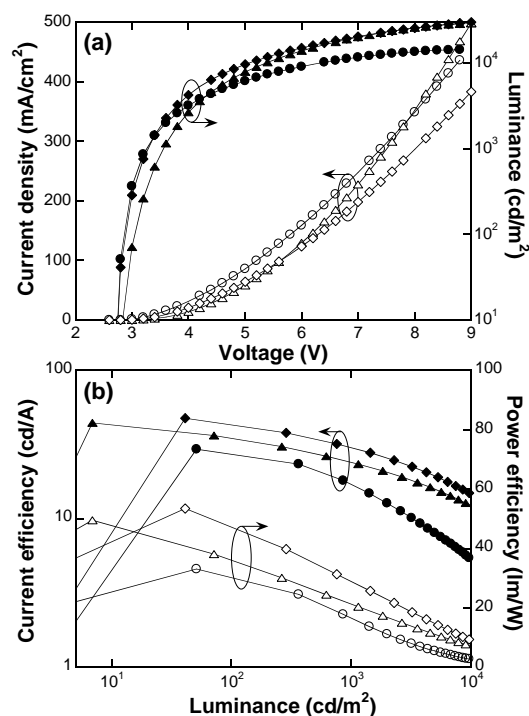


**Figure 4.** Current density and luminance versus driving voltage (a) and current efficiency and power efficiency versus luminance (b) characteristics of the F/P hybrid WOLEDs with TPA-PPI (○●), PPI-TPA-SO2-1(△▲), and PPI-TPA-SO2-2(◇◆) as the blue emitter as well as the host of PO-01 at 0.5 wt% doping concentration.

The typical EL spectra of the F/P hybrid WOLEDs at a current density of 1 mA cm<sup>-2</sup> are shown in Figure 5, and the EL spectra at different luminances are shown in Figure S11. All the EL spectra could be divided into their blue emission corresponding to the fluorophor host and yellow emission corresponding to the phosphor guest. The phosphorescence part contributes mostly to the emission for all the WOLEDs, indicating the efficiency of the phosphorescence emission should undoubtedly be the decisive factor for the F/P hybrid WOLEDs.

Transient PL spectra of the films doped with 0.5 wt% PO-01 were measured by time-correlated single photon counting method under the excitation of a nanosecond lamp ( $\lambda = 340$  nm) (Figure 6). The emission decay curves from the host detected at around 450 nm exhibit quite similar lifetimes in nanosecond level, indicating efficient singlet exciton radiative transition according to the kinetics function ( $k_r = \Phi/\tau$ ). The emission decay curves from the phosphor dopant detected at 560 nm resemble typical phosphorescence emission with long lifetimes in microsecond level. Except for the co-deposited film of PPI-TPA-SO2-1:PO-01 that gives a single exponential decay of phosphorescence with a lifetime of 1.22  $\mu$ s, TPA-PPI:PO-01 and PPI-TPA-SO2-2:PO-01 give double exponential decays of phosphorescence with lifetimes of 0.719/2.27 and 0.798/1.94  $\mu$ s, respectively. As  $T_1$  of TPA-PPI (2.23 eV) is only 0.02 eV higher than that of PO-01 (2.21 eV), the longest decay time (2.27  $\mu$ s) could originate from more easily reverse energy transfer from the dopant to the host. Longer lifetime impairs the device performance due to the bigger possibility of non-radiative transitions of the triplet excitons.<sup>21</sup> On the contrary, PPI-TPA-SO2-1 and PPI-

TPA-SO2-2 both with  $T_1$  of 2.30 eV exhibit shorter decay times and thus much better triplet exciton confining ability, and it could be the most important decisive factor of their F/P white device superiority.

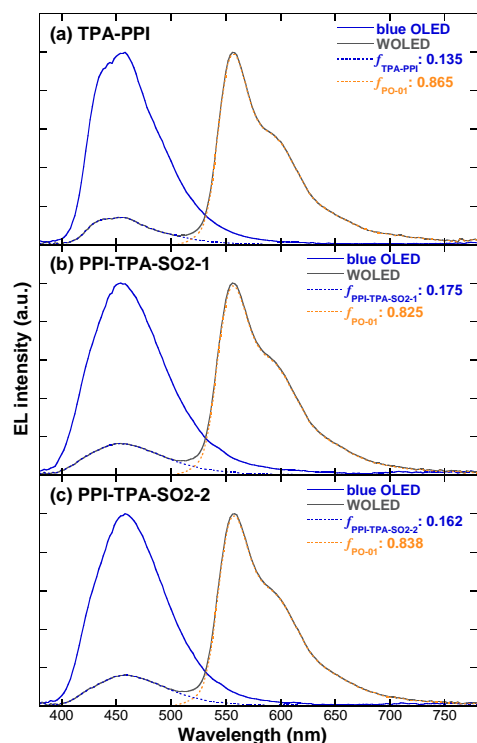


**Figure 5.** EL spectra of the blue OLEDs and the F/P hybrid WOLEDs based on TPA-PPI, PPI-TPA-SO2-1, and PPI-TPA-SO2-2 at a current density of  $1 \text{ mA cm}^{-2}$ . Also shown are the fitted emissions corresponding to the blue fluorophor (dashed blue lines) and the yellow phosphor PO-01 (dashed yellow lines).

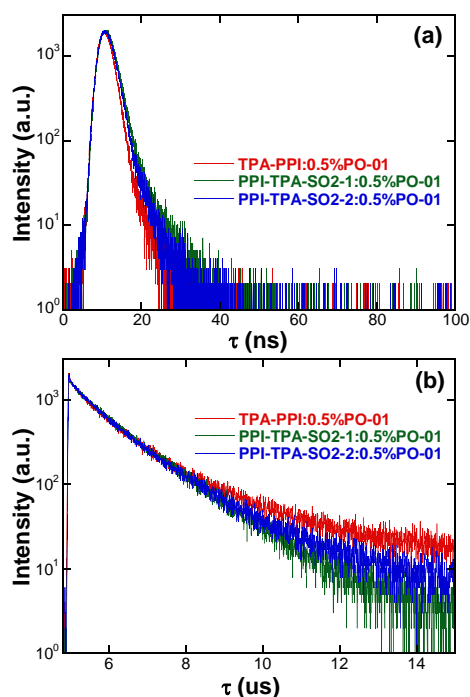


**Figure 6.** Transient PL decays of the co-deposited films of TPA-PPI:PO-1, PPI-TPA-SO2-1:PO-01, and PPI-TPA-SO2-2:PO-01 detected at 450 nm (a) and 560 nm (b).

As the single-EML architecture is free of spacer to separate the singlet and triplet excitons, the singlet and triplet exciton separation and utilization efficiency of the host itself would surely be even more important. The PL spectra of the neat films of TPA-PPI, PPI-TPA-SO2-1, and PPI-TPA-SO2-2 and their co-deposited films with 0.5 wt% PO-01 were utilized to investigate the energy-transfer mechanisms between the host and the dopant (Figure 7). As aforementioned, PLQY values of the neat films ( $\Phi_{neat}^{blue}$ ) are 0.84, 0.71, and 0.68 for TPA-PPI, PPI-TPA-SO2-1, and PPI-TPA-SO2-2, respectively. It is supposed only the host could be excited due to the extremely low doping concentration (0.5 wt%) of the dopant and all the generated excitons are singlet excitons under the photo exciting process. On the one hand, one part of the generated singlet excitons on the host would decay directly to give blue emission. On the other hand, the other part of the singlet exciton reaches PO-01 to give yellow emission. Similarly, PLQY values of the doped films ( $\Phi_{doped}^{white}$ ) are measured to be 0.86, 0.94, and 0.97 for TPA-PPI, PPI-TPA-SO2-1, and PPI-TPA-SO2-2, respectively. As shown in Figure 7, the respective blue and yellow emission proportions were calculated according to the integrations of the fitted corresponding emission spectra for the host and the guest. The contribution of the blue fluorescence ( $\Phi_{doped}^{blue}$ ) for PLQYs of the doped films are 0.104, 0.162, and 0.147 for the doped films of TPA-PPI, PPI-TPA-SO2-1, and PPI-TPA-SO2-2, respectively, as estimated by the following equation (3):

$$\Phi_{doped}^{blue} = \Phi_{doped}^{white} \times f_{blue} \quad (3),$$

where  $f_{blue}$  is the contents of the blue emission from the host. Similarly, the contribution of the yellow phosphorescence ( $\Phi_{doped}^{yellow}$ ) for PLQYs of the doped films are estimated to be 0.756, 0.778, and

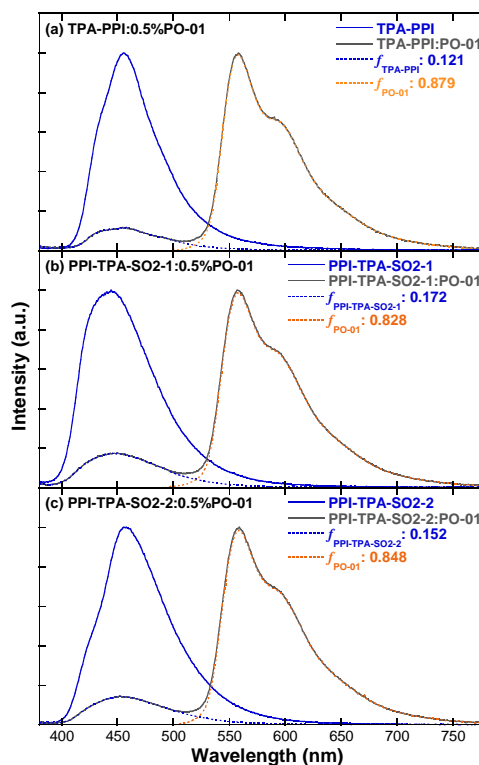


**Figure 7.** PL spectra of the neat films of TPA-PPI, PPI-TPA-SO2-1, and PPI-TPA-SO2-2 and their co-deposited films with PO-01 at a doping concentration of 0.5 wt% excited at 340 nm. Also shown are the fitted emissions corresponding to the host (blue dashed lines) and the phosphor (yellow dashed lines).

**Table 4.** Summary of the experimental and fitted photoluminescent emissions of the co-deposited films for TPA-PPI:PO-1, PPI-TPA-SO2-1:PO-01, and PPI-TPA-SO2-2:PO-01.

View Article Online  
DOI: 10.1039/C5TC01373A

host	$\Phi_{neat}^{blue}$	$\Phi_{doped}^{white}$	$\Phi_{doped}^{blue}$	$\Phi_{doped}^{yellow}$	$\Phi_{doped}^{blue}/\Phi_{neat}^{blue}$	$x_{trans}^{photo}$
TPA-PPI	0.84	0.86	0.104	0.756	0.124	0.876
PPI-TPA-SO2-1	0.71	0.94	0.162	0.778	0.228	0.772
PPI-TPA-SO2-2	0.68	0.97	0.147	0.823	0.216	0.784

0.823 for the doped films of TPA-PPI, PPI-TPA-SO2-2, and PPI-TPA-SO2-1, respectively according to equation (4):

$$\Phi_{doped}^{yellow} = \Phi_{doped}^{white} \times f_{yellow} \quad (4),$$

where  $f_{yellow}$  is the contents of the yellow emission from the guest. The fraction of the singlet excitons transferred to the dopant ( $x_{trans}^{photo}$ ) under the photo exciting process could be defined as the following equation (6):

$$\Phi_{doped}^{blue} = \Phi_{neat}^{blue} (1 - x_{trans}^{photo}) \quad (5),$$

$$x_{trans}^{photo} = 1 - \Phi_{doped}^{blue} / \Phi_{neat}^{blue} \quad (6).$$

The  $x_{trans}^{photo}$  values calculated for the doped films of TPA-PPI, PPI-TPA-SO2-1, and PPI-TPA-SO2-2 are 0.876, 0.772, and 0.784, respectively, as shown in Table 4. It indicates a larger amount of singlet excitons is transferred to the dopant to suppress the blue emission of the host TPA-PPI itself compared with PPI-TPA-SO2-1 and PPI-TPA-SO2-2. However, the captured excitons by the phosphor dopant could not decay efficiently as they contribute the smallest yellow phosphorescence content for PLQY. The doped films of PPI-TPA-SO2-1 and PPI-TPA-SO2-2 exhibit higher efficiency than the doped film of TPA-PPI for both the blue and yellow emission parts even though their neat film PLQY values are inferior to TPA-PPI. Especially for PPI-TPA-SO2-2, the  $\Phi_{doped}^{yellow}$  value is even larger than the  $x_{trans}^{photo}$  value, indicating some of the exciton energy which nonradiatively decays in the neat film of PPI-TPA-SO2-2 could even be transferred to the phosphor dopant in the co-deposited film to give radiative decay (Figure 8). Benefited from better triplet exciton confining ability, although less amount of singlet excitons transfers to PO-01, more photons can be released for the systems of PPI-TPA-SO2-1 and PPI-TPA-SO2-2, indicating both PPI-TPA-SO2-1 and PPI-TPA-SO2-2 have superior singlet and triplet exciton separation and utilization ability as a host. In comparison, the defect of TPA-PPI as a host could even be amplified due to a larger portion of 75% triplet excitons initially generated in an electroluminescent process. Lower singlet and triplet exciton separation and utilization ability would cause greater exciton waste and lower efficiency for the F/P hybrid WOLEDs based on TPA-PPI compared with PPI-TPA-SO2-1 and PPI-TPA-SO2-2. And the performance difference between the devices based on PPI-TPA-SO2-1 and PPI-TPA-SO2-2 are in accordance to the trend of their

corresponding PLQY values.

Meanwhile, the singlet and triplet excitons could be transferred to the dopant, and the carriers might also be captured by the dopant to generate excitons directly in the electroluminescent process. The EQE variation of the WOLEDs could be affected by such process as well. As shown in Table 5, at a typical current density of 1 mA cm<sup>-2</sup>, the EQE values of the F/P hybrid WOLEDs ( $\eta_{White}$ ) are 7.84%, 10.5%, and 12.8% for the devices based on TPA-PPI, PPI-TPA-SO2-1, and PPI-TPA-SO2-2, respectively. The EL spectra of the WOLEDs can also be divided into those from the fluorophor host and the phosphor guest (Figure 5). It is of interest the contents of the blue and yellow emissions in EL spectra are almost the same as those in PL spectra (Figure 7), indicating most of the carriers are recombined on the host molecules and the yellow electroluminescent emission could be attributed to the energy transfer from the host to the guest. According to the fitted results, the contributions of the blue fluorescence emission ( $\eta_{Blue}^{F-P}$ ) to the EQE values of the WOLEDs are 1.06%, 1.84%, and 2.07%, and the contributions of the yellow phosphorescence emission ( $\eta_{Yellow}^{F-P}$ ) are 6.78%, 8.66%, and 10.73% for the devices based on TPA-PPI, PPI-TPA-SO2-1, and PPI-TPA-SO2-2, respectively.

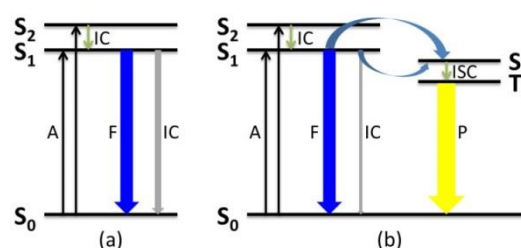


**Figure 8.** A schematic diagram for the photoluminescence process of (a) the neat films of PPI-TPA-SO2-1 and PPI-TPA-SO2-2 and (b) the co-deposited films with PO-01 at a doping concentration of 0.5 wt% excited at 340 nm. Part of the singlet excited energy that is nonradiatively decayed in the neat film is transferred to the PO-01 dopant to give phosphorescence and reduced nonradiative transition. A: absorption, F: fluorescence, IC: internal conversion, P: phosphorescence, and ISC: intersystem conversion.

On the assumption that the WOLEDs have the same optical out-coupling factor ( $\eta_{op}$ ) and carrier balance factor ( $\gamma$ ) as the nondoped blue OLEDs, the singlet excitons contributed to the blue

**Table 5.** Summary of the experimental and fitted electroluminescent emissions of the F/P hybrid WOLEDs based on TPA-PPI, PPI-TPA-SO2-1, and PPI-TPA-SO2-2 at 1 mA cm<sup>-2</sup>.

host	$\eta_{Blue}$ (%)	$\eta_{White}$ (%)	$\eta_{Blue}^{F-P}$ (%)	$\eta_{Yellow}^{F-P}$ (%)	$\eta_{Blue}^S$ (%)	$\eta_{Blue}^{S+T}$ (%)	$\eta_{Yellow}^{S+T}$ (%)
TPA-PPI	4.11	7.84	1.06	6.78	25.8	6.45	93.55
PPI-TPA-SO2-1	3.34	10.5	1.84	8.66	54.8	13.7	86.3
PPI-TPA-SO2-2	4.54	12.8	2.07	10.73	45.8	11.45	88.55

electroluminescence among all the electro-generated singlet excitons ( $\eta_{Blue}^S$ ) is only 25.8% for the WOLED based on TPA-PPI (Table 5), as estimated by the following equation (7):

$$\eta_{Blue}^S = \eta_{Blue}^{F-P} / \eta_{Blue} \quad (7),$$

where  $\eta_{Blue}$  is the EQE value of the nondoped blue fluorescent device. Considering 25% of the excitons are singlet excitons in the electroluminescent process, the excitons contributed to the blue electroluminescence ( $\eta_{Blue}^{S+T}$ ) among all the electro-generated excitons is only 6.45%. The rest of the excitons ( $\eta_{Yellow}^{S+T}=93.55\%$ ) may contribute to the yellow electroluminescent emission or nonradiatively decays to the ground state. It is of interest the  $\eta_{Blue}^{S+T}$  values for the WOLEDs based on PPI-TPA-SO2-1 (13.7%) and PPI-TPA-SO2-2 (11.45%) are almost two times larger than that of the device based on TPA-PPI (6.45%). The relatively lower  $\eta_{Blue}^{S+T}$  value for the device based on TPA-PPI further indicates the phosphorescent dopant in TPA-PPI may suppress the blue emission from TPA-PPI through energy transfer and/or nonradiative quenching. Although the  $\eta_{Yellow}^{S+T}$  values for the devices based on PPI-TPA-SO2-1 (86.3%) and PPI-TPA-SO2-2 (88.55%) are lower than that of the device based on TPA-PPI (93.55%), their contributions to the yellow phosphorescence emission ( $\eta_{Yellow}^{F-P}$ ) are much higher than the device based on TPA-PPI. It further proves their superior singlet and triplet exciton separation and utilization ability over TPA-PPI.

Last but not the least, the carrier injection and transporting ability would unavoidably affect the carrier recombination efficiency and thus the device performance. In order to investigate the potential effect of the phosphor dopant on the carrier transporting ability, hole-only and electron-only devices were also fabricated at a doping concentration of 0.5 wt%. The configuration of the hole-only devices is ITO (95 nm)/ HATCN (5 nm)/ NPB (40 nm)/ TCTA (5 nm)/ TPA-PPI, PPI-TPA-SO2-1 or PPI-TPA-SO2-2: 0.5 wt% PO-01 (20 nm)/ NPB (30 nm)/ Au (80 nm), and the electron-only devices have a structure of ITO (95 nm)/ TPBI (45 nm)/ TPA-PPI, PPI-TPA-SO2-1 or PPI-TPA-SO2-2: 0.5 wt% PO-01 (20 nm)/ TPBI (40 nm)/ LiF (1 nm)/ Au (80 nm). As shown in Figure S12, similar to the nondoped carrier-only devices, the TPA-PPI based devices show the biggest hole current, and its hole current surpasses its electron current, indicating its hole dominant transporting property. In contrast, the electron current of the devices based on PPI-TPA-SO2-1 and PPI-TPA-SO2-2 is larger than the hole current due to the lower electron injection barrier from the ETL of TPBI to the active layer. The similar tendency in hole and electron current of the nondoped and doped devices further indicates most of the carriers should be transported and recombined on the host molecules and then part of the exciton energy could be transferred to the phosphor guest to give complementary yellow emission.

## Conclusions

In summary, two novel isomeric deep blue fluorophors of PPI-TPA-SO2-1 and PPI-TPA-SO2-2 combined with PPI and sulfone-locked TPA were designed and synthesized. The sulfone lock induces larger twisted angles between PPI and sulfone-locked TPA, thus higher triplet energy levels and better triplet exciton confining ability compared with their analogue TPA-PPI without the sulfone lock. In addition, different from the hole dominant transporting property of TPA-PPI, the sulfone-locked analogues exhibit electron dominant transporting property to give more balanced carriers. Thus, the F/P hybrid WOLEDs based on PPI-TPA-SO2-1 and PPI-TPA-SO2-2 as the host of yellow phosphor as well as the blue emitter achieved maximum forward-viewing current efficiencies of 44.2 and 47.6 cd A<sup>-1</sup>, power efficiencies of 49.5

and 53.4 lm W<sup>-1</sup>, and EQE values of 14.4% and 15.6%. Both are significantly improved because of their superior singlet and triplet exciton separation and utilization ability over TPA-PPI, as proved by the energy-transfer in both the photoluminescent and electroluminescent processes. The current values are also hitherto the highest efficiency for the F/P hybrid WOLEDs in a single-EML architecture. The current findings also provide instructive insight into the molecular design of blue fluorophor and host for F/P hybrid WOLED applications.

## EXPERIMENTAL SECTION

### Measurements and characterization

<sup>1</sup>H and <sup>13</sup>C NMR spectra were measured on a Bruker NMR spectrometer operating at 600 and 150 MHz, respectively, in deuterated chloroform (CDCl<sub>3</sub>) solution at room temperature. Differential scanning calorimetry (DSC) measurements were operated on a Netzsch DSC 209 under a N<sub>2</sub> flow at a heating and cooling rate of 10 °C min<sup>-1</sup>. Thermogravimetric analyses (TGA) were recorded on a Netzsch TG 209 under a N<sub>2</sub> flow at a heating rate of 10 °C min<sup>-1</sup>. UV-vis absorption spectra were recorded on a HP 8453 spectrophotometer. Photoluminescence (PL) spectra were measured using a Jobin-Yvon spectrofluorometer. Cyclic voltammetry (CV) was performed on a CHI600D electrochemical work station with a Pt working electrode and a Pt wire counter electrode at a scanning rate of 100 mV s<sup>-1</sup> against a Ag/Ag<sup>+</sup> (0.1 M of AgNO<sub>3</sub> in acetonitrile) reference electrode with a nitrogen-saturated anhydrous acetonitrile and dichloromethane (DCM) solution of 0.1 mol L<sup>-1</sup> tetrabutylammonium hexafluorophosphate. PL quantum yields (PLQYs) in solution and film were measured by using an integrating sphere on a HAMAMATSU absolute PL quantum yield spectrometer C11347. Transient PL was measured with an Edinburgh FL920 fluorescence spectrophotometer. The thin solid films used for absorption and PL spectral measurement were vacuum vapor deposited on quartz substrates. Matrix-assisted laser-desorption/ionization time-of-flight (MALDI-TOF) mass spectra were recorded on a Bruker BIFLEXIII TOF mass spectrometer.

### Theoretical Calculation

Density functional theory (DFT) calculations were performed on B3LYP/6-31G(d, p) basis set based on Gaussian suite of programs (Gaussian 03W).<sup>17</sup> Spatial distributions of the HOMOs and LUMOs of the compounds were obtained from the optimized ground state structures. The M06-2X functional, which is well-known for intermediate description of the charge-transfer systems, was utilized to gain further insight into the character of the excited states. Based on the optimized structures of the ground states, the excited singlet energy (E<sub>S</sub>) and triplet energy (E<sub>T</sub>) were further calculated to investigate the split energy ( $\Delta E_{ST}$ ) between E<sub>S</sub> and E<sub>T</sub>.

### Device Fabrication and Characterization

Glass substrates pre-coated with a 95 nm thin layer of indium tin oxide (ITO) with a sheet resistance of 10 Ω per square were carefully cleaned by acetone, isopropyl alcohol, detergent, deionized water, and isopropyl alcohol under ultrasonic bath and treated with O<sub>2</sub> plasma for 20 min in sequence. Organic layers were deposited onto the ITO-coated glass substrates by thermal evaporation under high vacuum (<5×10<sup>-4</sup> Pa). Cathode, consisting of a 1 nm thin layer of LiF followed by a 90 nm thin layer of Al, was patterned using a shadow mask with an array of 3 mm×3 mm openings. Deposition rates are kept at 1~2 Å/s for organic materials, 0.1 Å/s for LiF, and 6 Å/s for Al. Electroluminescence (EL) spectra were measured by an optical analyzer, Photo Research PR705. The current density and luminance versus driving voltage were detected by Keithley 2420 and Konica Minolta chromameter CS-200. EQE was calculated from

the luminance, current density, and EL spectrum on the premise of a Lambertian distribution.

## Materials

All solvents and reagents were used as received from commercial suppliers without further purification. 10-Phenyl-10H-phenothiazine (**4**)<sup>15a</sup> and 1-phenyl-2-(4-(4,4,5,5-tetramethyl-1,3,2-dioxaborolan-2-yl)phenyl)-1H-phenanthro[9,10-d]imidazole (**7**)<sup>15b</sup> were synthesized according to the literature procedures. Synthetic routes of the intermediates and the target compounds PPI-TPA-SO2-1 and PPI-TPA-SO2-2 are outlined in Scheme 1. TPA-PPI was synthesized according to the reported procedures.<sup>12b</sup> The developed target materials were further purified by repeated temperature gradient vacuum sublimation.

**10-(4-bromophenyl)-10H-phenothiazine (2).** Phenothiazine (3.98 g, 20 mmol) in dry N,N-dimethylformamide (DMF) (60 mL) was stirred under argon. 1,4-Bromiodobenzene (8.46 g, 30 mmol, 1.5 equiv) was added with vigorous stirring. Then copper powder (1.3 g, 20 mmol) was added. The reaction mixture was stirred at 160 °C under the protection of nitrogen gas. After stirred for 48 h, the reaction mixture was extracted with dichloromethane (DCM) and further purified by column chromatography to afford **2** (3.82 g, yield 54%) as a white solid. <sup>1</sup>H NMR (600 MHz, CDCl<sub>3</sub>, δ, ppm): 7.71 (d, *J* = 7.3 Hz, 2H), 7.26 (s, 4H), 7.04 (d, *J* = 8.9 Hz, 2H), 6.88 (s, 2H), 6.25 (s, 2H).

**10-(4-bromophenyl)-10H-phenothiazine-S,S-dioxide (3).** A mixture of **2** (7.06 g, 20 mmol), 90 mL of DCM, 45 mL of AcOH, 5.2 mL of H<sub>2</sub>O<sub>2</sub> (100 mmol, 2.5 equiv) was stirred under atmosphere at 80 °C for 24 h. The reaction mixture was extracted with DCM and further purified by column chromatography to afford **3** (6.21 g, yield 88%) as a white solid. <sup>1</sup>H NMR (600 MHz, CDCl<sub>3</sub>, δ, ppm): 8.20 (dd, *J* = 7.9 and 1.3 Hz, 2H), 7.86 (d, *J* = 8.5 Hz, 2H), 7.51-7.35 (m, 2H), 7.35-7.20 (m, 4H), 6.64 (d, *J* = 8.6 Hz, 2H).

**3-bromo-10-phenyl-10H-phenothiazine (5).** 10-Phenyl-10H-phenothiazine (**4**) (5.5 g, 20 mmol) was dissolved in 80 mL of DCM. Bromine (4.8 g, 30 mmol, 1.5 equiv) was added slowly with ice bath, and the ice bath was removed after the addition of bromine. The reaction mixture was stirred at room temperature for 5 h. After the reaction, the residual bromine was quenched by NaHSO<sub>3</sub>, and the reaction mixture was extracted by DCM. The solvent was removed by vacuum distillation to give a brown oil (6.2 g). The product is a mixture containing **5** and could not be purified and was used directly for the next step.

**3-bromo-10-phenyl-10H-phenothiazine-S,S-dioxide (6).** The brown oil mixture (6.2 g) was dissolved in a mixture of 90 mL of DCM, 45 mL of AcOH, and 4.8 mL of H<sub>2</sub>O<sub>2</sub>, and was stirred under atmosphere at 80 °C for 24 h. The reaction mixture was extracted with DCM and further purified by column chromatography to afford **6** (2.3 g) as a white solid. <sup>1</sup>H NMR (600 MHz, CDCl<sub>3</sub>, δ, ppm): 8.20-8.22 (s, 1H), 8.19-8.18 (d, *J* = 7.8 Hz, 1H), 7.86-7.84 (m, 1H), 7.84-7.78 (m, 2H), 7.28-7.48 (m, 5H), 6.62-6.64 (d, *J* = 8.5 Hz, 2H), 6.48-6.52 (d, *J* = 7.2 Hz, 2H).

**10-(4-(2'-(1'-phenyl)-1'-phenyl-1'H-phenanthro[9',10'-d]imidazolephenyl)-10H-phenothiazine-S,S-dioxide (PPI-TPA-SO2-I).** Toluene (60 mL), ethanol (20 mL), and 2 M aqueous Na<sub>2</sub>CO<sub>3</sub> (15 mL) were added to a mixture of **3** (0.76 g, 2 mmol), **7** (0.99 g, 2.0 mmol), and Pd(PPh<sub>3</sub>)<sub>4</sub> (52 mg, 3 mol%). The suspension was stirred at 90 °C for 24 h under a nitrogen atmosphere. When cooled to room temperature, the mixture was extracted with CH<sub>2</sub>Cl<sub>2</sub> and dried over Na<sub>2</sub>SO<sub>4</sub>. After the removal of solvent, the residue was purified by column chromatography on silica gel to afford PPI-TPA-SO2-1 (1.1 g, yield 88%) as a white solid. <sup>1</sup>H NMR (600 MHz, CDCl<sub>3</sub>, δ, ppm): 8.77 (dd, *J* = 20.0 and 8.3 Hz, 2H), 8.19 (dd, *J* = 7.9 and 1.4 Hz,

2H), 7.90 (d, *J* = 8.4 Hz, 2H), 7.84-7.49 (m, 11H), 7.52-7.34 (m, 4H), 7.33-7.23 (m, 6H), 6.70 (d, *J* = 8.6 Hz, 2H). <sup>13</sup>C NMR (150 MHz, CDCl<sub>3</sub>, δ, ppm): 140.73, 132.80, 130.90, 130.35, 130.08, 129.81, 129.12, 127.01, 124.20, 123.47, 123.17, 122.69, 122.13, 120.91, 117.21, 77.23, 77.02, 76.81. MS (MALDI-TOF): *m/z* calcd for C<sub>45</sub>H<sub>29</sub>N<sub>3</sub>O<sub>2</sub>S: 675.2; found: 676.188. Anal. Calcd. for C<sub>45</sub>H<sub>29</sub>N<sub>3</sub>O<sub>2</sub>S: C, 79.98; H, 4.33; N, 6.22; O, 4.73; S, 4.74. Found: C, 79.88; H, 4.53; N, 6.14; S, 4.46

**3-2'-(1'-phenyl)-1'-phenyl-1'H-phenanthro[9',10'-d]imidazole-10-phenyl-10H-phenothiazine-S,S-dioxide (PPI-TPA-SO2-2).** PPI-TPA-SO2-2 (1.02 g, yield 76%) was synthesized as a white solid in a similar manner of PPI-TPA-SO2-1 with **6** instead of **3**. <sup>1</sup>H NMR (600 MHz, CDCl<sub>3</sub>, δ, ppm): 8.89 (d, *J* = 7.8 Hz, 1H), 8.74 (dd, *J* = 37.9 and 8.4 Hz, 2H), 8.36 (d, *J* = 2.2 Hz, 1H), 8.19 (dd, *J* = 7.9 and 1.4 Hz, 1H), 7.77-7.60 (m, 11H), 7.53 (m, 5H), 7.39 (m, 3H), 7.26-7.19 (m, 3H), 6.65 (dd, *J* = 27.1 and 8.8 Hz, 2H). <sup>13</sup>C NMR (151 MHz, CDCl<sub>3</sub>, δ, ppm): 140.59, 139.97, 138.82, 134.26, 132.84, 131.40, 131.15, 130.34, 129.90, 129.31, 129.10, 128.29, 127.30, 126.34, 125.65, 124.93, 124.11, 123.50, 123.11, 122.92, 122.76, 122.19, 121.35, 120.90, 117.87, 117.26, 77.22, 77.01, 76.80. MS (MALDI-TOF): *m/z* calcd for C<sub>45</sub>H<sub>29</sub>N<sub>3</sub>O<sub>2</sub>S: 675.2; found: 676.178. Anal. Calcd. for C<sub>45</sub>H<sub>29</sub>N<sub>3</sub>O<sub>2</sub>S: C, 79.98; H, 4.33; N, 6.22; O, 4.73; S, 4.74. Found: C, 79.85; H, 4.51; N, 6.13; S, 4.58

## Acknowledgements

The authors greatly appreciate the financial support from the Ministry of Science and Technology (2015CB655003 and 2014DFA52030), the National Natural Science Foundation of China (91233116 and 51073057), the Ministry of Education (NCET-11-0159), and the Guangdong Natural Science Foundation (S2012030006232). The authors are grateful to Liang Yao for his help in low temperature phosphorescence measurements.

## Notes and references

- C. W. Tang, S. VanSlyke, *A. Appl. Phys. Lett.*, 1987, **51**, 913.
- (a) B. W. D'Andrade, S. R. Forrest, *Adv. Mater.*, 2004, **16**, 1585. (b) J. H. Burroughes, D. D. C. Bradley, A. R. Brown, R. N. Marks, K. Mackay, R. H. Friend, P. L. Burn, A. B. Holmes, *Nature*, 1990, **347**, 539. (c) M. A. Baldo, M. E. Thompson, S. R. Forrest, *Nature*, 2000, **403**, 750. (d) S.-J. Su, E. Gonmori, H. Sasabe, Kido, *J. Adv. Mater.*, 2008, **20**, 4189. (e) Y. T. Tao, C. L. Yang, J. G. Qin, *Chem. Soc. Rev.*, 2011, **40**, 2943.
- S. Reineke, F. Lindner, G. Schwartz, N. Seidler, K. Leo, *Nature*, 2009, **459**, 234.
- S. J. Yeh, M. F. Wu, C. T. Chen, Y. H. Song, Y. Chi, M. H. Ho, *Adv. Mater.*, 2005, **17**, 285.
- (a) Y. Sun, N. C. Giebink, H. Kanno, B. Ma, M. E. Thompson, S. R. Forrest, *Nature*, 2006, **440**, 908. (b) T. Peng, Y. Yang, H. Bi, Y. Liu, Z. Hou, Y. Wang, *J. Mater. Chem.*, 2011, **21**, 3551.
- J. Ye, Z. Chen, F. F. An, M. L. Sun, H.-W. Mo, X. H. Zhang, C.-S. Lee, *Appl. Mater. Interfaces*, 2014, **6**, 8964.
- (a) S. R. Forrest, *Nature*, 2004, **428**, 911. (b) J. S. Huang, G. Li, E. Wu, Q. F. Xu, Y. Yang, *Adv. Mater.*, 2006, **18**, 114. (c) M. C. Gather, A. Kohnen, K. Meerholz, *Adv. Mater.*, 2011, **23**, 233.
- Y. T. Tao, C. L. Yang, J. G. Qin, *Chem. Soc. Rev.*, 2011, **40**, 2943.
- (a) G. Schwartz, M. Pfeiffer, S. Reineke, K. Walzer, K. Leo, *Adv. Mater.*, 2007, **19**, 3672. (b) Y. T. Tao, Q. Wang, Y. Shang, C. L. Yang, L. Ao, J. G. Qin, D. G. Ma, Z. G. Shuai, *Chem.*

- Commun.*, 2009, **77**. (c) W. Y. Hung, L.-C. Chi, W.-J. Chen, Y.-M. Chen, S.-H. Chou, K.-T. Wong, *J. Mater. Chem.*, 2010, **20**, 10113.
10. C. Adachi, M. A. Baldo, M. E. Thompson, S. R. Forrest, *J. Appl. Phys.*, 2001, **90**, 5048
11. J. Ye, C.-J. Zheng, X.-M. Ou, X.-H. Zhang, M.-K. Fung, C.-S. Lee, *Adv. Mater.*, 2012, **24**, 3410.
12. (a) C.-H. Chen, W.-S. Huang, M.-Y. Lai, W.-C. Tsao, J. T. Lin, Y.-H. Wu, T.-H. Ke, L.-Y. Chen, C.-C. Wu, *Adv. Funct. Mater.*, 2009, **19**, 2661. (b) W. Li, D. D. Liu, F. Z. Shen, D. G. Ma, Z. M. Wang, T. Feng, Y. X. Xu, B. Yang, Y. G. Ma, *Adv. Funct. Mater.*, 2012, **22**, 2797. (c) Y. Zhang, S.-L. Lai, Q.-X. Tong, M.-F. Lo, T.-W. Ng, M.-Y. Chan, Z.-C. Wen, J. He, K.-S. Jeff, X.-L. Tang, W.-M. Liu, C.-C. Ko, P.-F. Wang, C.-S. Lee, *Chem. Mater.*, 2012, **24**, 61.
13. H. Sasabe, Y. Seino, M. Kimura, J. Kido. *Chem. Mater.*, 2012, **24**, 1404.
14. D. Zhang, L. Duan, Y. Li, D. Zhang, Y. Qiu, *J. Mater. Chem. C*, 2014, **2**, 8191.
15. (a) D. L. Sun, S. V. Rosokha, J. K. Kochi, *J. Am. Chem. Soc.* 2004, **126**, 1388. (b) H. Liu, P. Chen, D. H. Hu, X. Y. Tang, Y. Y. Pan, H. H. Zhang, W. Q. Zhang, X. Han, Q. Bai, P. Lu, Y. G. Ma, *Chem. Eur. J.*, 2014, **20**, 2149.
16. (a) Y. Seino, H. Sasabe, Y.-J. Pu, J. Kido, *Adv. Mater.*, 2014, **26**, 1612.
17. J.-L. Bredas, *Mater. Horiz.*, 2014, **1**, 17.
18. Gaussian 03, Revision D.01, M. J. Frisch, G. W. Trucks, H. B. Schlegel, G. E. Scuseria, M. A. Robb, J. R. Cheeseman, J. A. Montgomery, T. Vreven, K. N. Kudin, J. C. Burant, J. M. Millam, S. S. Iyengar, J. Tomasi, V. Barone, B. Mennucci, M. Cossi, G. Scalmani, N. Rega, G. A. Petersson, H. Nakatsuji, M. Hada, M. Ehara, K. Toyota, R. Fukuda, J. Hasegawa, M. Ishida, T. Nakajima, Y. Honda, O. Kitao, H. Nakai, M. Klene, X. Li, J. E. Knox, H. P. Hratchian, J. B. Cross, V. Bakken, C. Adamo, J. Jaramillo, R. Gomperts, R. E. Stratmann, O. Yazyev, A. J. Austin, R. Cammi, C. Pomelli, J. W. Ochterski, P. Y. Ayala, K. Morokuma, G. A. Voth, P. Salvador, J. J. Dannenberg, V. G. Zakrzewski, S. Dapprich, A. D. Daniels, M. C. Strain, O. Farkas, D. K. Malick, A. D. Rabuck, K. Raghavachari, J. B. Foresman, J. V. Ortiz, Q. Cui, A. G. Baboul, S. Clifford, J. Cioslowski, B. B. Stefanov, G. Liu, A. Liashenko, P. Piskorz, I. Komaromi, R. L. Martin, D. J. Fox, T. Keith, M. A. Al-Laham, C. Y. Peng, A. Nanayakkara, M. Challacombe, P. M. W. Gill, B. Johnson, W. Chen, M. W. Wong, C. Gonzalez, J. A. Pople, Gaussian, Inc., Wallingford CT, 2004.
19. (a) Q. S. Zhang, J. Li, K. Shizu, S. P. Huang, S. Hirata, H. Miyazaki, C. Adachi, *J. Am. Chem. Soc.*, 2012, **134**, 14706. (b) F. B. Dias, K. N. Bourdakos, V. Jankus, K. C. Moss, K. T. Kamtekar, V. Bhalla, J. Santos, M. R. Bryce, A. P. Monkman, *Adv. Mater.*, 2013, **25**, 3707.
20. W. J. Li, Y. Y. Pan, R. Xiao, Q. M. Peng, S. T. Zhang, D. G. Ma, F. Li, F. Z. Shen, Y. H. Wang, B. Yang, Y. G. Ma, *Adv. Funct. Mater.*, 2014, **24**, 1609.
21. S.-J. Su, Y. Takahashi, T. Chiba, T. Takeda, J. Kido, *Adv. Funct. Mater.*, 2009, **19**, 1260.

**Table of Contents entry:**

Deep blue fluorophors incorporated sulfone-locked triphenylamine were developed for highly efficient fluorescence/phosphorescence hybrid white OLEDs.

